ISSN 1674-1056
http://cpb.iphy.ac.cn
http://iopscience.iop.org/cpb
中国物理 B
Chinese Physics
中国物理 Chinese Physics B

Magnetostructural transformation and magnetocaloric effect in $Mn_{48-x}V_xNi_{42}Sn_{10}$ ferromagnetic shape memory alloys

Najam ul Hassan, Ishfaq Ahmad Shah, Tahira Khan, Jun Liu(刘俊), Yuanyuan Gong(龚元元), Xuefei Miao(缪雪飞), Feng Xu(徐锋)
Citation: Chin. Phys. B . 2018, 27(3): 037504. **doi:** 10.1088/1674-1056/27/3/037504

Journal homepage: http://cpb.iphy.ac.cn; http://iopscience.iop.org/cpb

What follows is a list of articles you may be interested in

Magnetocaloric effect in the layered organic-inorganic hybrid $(CH_3NH_3)_2CuCl_4$

Yinina Ma(马怡妮娜), Kun Zhai(翟昆), Liqin Yan(闫丽琴), Yisheng Chai(柴一晟), Dashan Shang(尚大山), Young Sun(孙阳)
Chin. Phys. B . 2018, 27(2): 027501. **doi:** 10.1088/1674-1056/27/2/027501

Influences of La and Ce doping on giant magnetocaloric effect of EuTiO

Zhao-Jun Mo(莫兆军), Qi-Lei Sun(孙启磊), Jun Shen(沈俊), Mo Yang(杨墨), Yu-Jin Li(黎玉进), Lan Li(李岚), Guo-Dong Liu(刘国栋), Cheng-Chun Tang(唐成春), Fan-Bin Meng(孟凡斌)
Chin. Phys. B . 2018, 27(1): 017501. **doi:** 10.1088/1674-1056/27/1/017501

Influence of Ni/Mn ratio on magnetostructural transformation and magnetocaloric effect in $Ni_{48-x}Co_2Mn_{38+x}Sn_{12}$ (x = 0, 1.0, 1.5, 2.0, and 2.5) ferromagnetic shape memory alloys

Ishfaq Ahmad Shah, Najam ul Hassan, Abdur Rauf, Jun Liu(刘俊), Yuanyuan Gong(龚元元), Guizhou Xu(徐桂舟), Feng Xu(徐锋)
Chin. Phys. B . 2017, 26(9): 097501. **doi:** 10.1088/1674-1056/26/9/097501

Magnetic properties and magnetocaloric effect of the Cr-based spinel sulfides $Co_{1-x}Cu_xCr_2S_4$

Xiao-Chao Zheng(郑小超), Xi-Yang Li(李西阳), Lun-Hua He(何伦华), Shao-Ying Zhang(张绍英), Ming-Hua Tang(唐明华), Fang-Wei Wang(王芳卫)
Chin. Phys. B . 2017, 26(3): 037502. **doi:** 10.1088/1674-1056/26/3/037502

Effect of Sb-doping on martensitic transformation and magnetocaloric effect in Mn-rich $Mn_{50}Ni_{40}Sn_{10-x}Sb_x$ (x=1, 2, 3, and 4) alloys

Ishfaq Ahmad Shah, Najam ul Hassan, Jun Liu(刘俊), Yuanyuan Gong(龚元元), Guizhou Xu(徐桂舟), Feng Xu(徐锋)
Chin. Phys. B . 2017, 26(1): 017501. **doi:** 10.1088/1674-1056/26/1/017501

Magnetostructural transformation and magnetocaloric effect in $Mn_{48-x}V_xNi_{42}Sn_{10}$ ferromagnetic shape memory alloys*

Najam ul Hassan[1], Ishfaq Ahmad Shah[1], Tahira Khan[2], Jun Liu(刘俊)[1], Yuanyuan Gong(龚元元)[1], Xuefei Miao(缪雪飞)[1], and Feng Xu(徐锋)[1,†]

[1] *MIIT Key Laboratory of Advanced Metallic and Intermetallic Materials Technology, School of Materials Science and Engineering, Nanjing University of Science and Technology, Nanjing* 210094, *China*

[2] *Beijing National Laboratory for Condensed Matter Physics, Chinese Academy of Sciences, Beijing* 100190, *China*

(Received 29 October 2017; revised manuscript received 19 December 2017; published online 13 February 2018)

In this work, we tuned the magnetostructural transformation and the coupled magnetocaloric properties of $Mn_{48-x}V_xNi_{42}Sn_{10}$ ($x = 0$, 1, 2, and 3) ferromagnetic shape memory alloys prepared by means of partial replacement of Mn by V. It is observed that the martensitic transformation temperatures decrease with the increase of V content. The shift of the transition temperatures to lower temperatures driven by the applied field, the metamagnetic behavior, and the thermal hysteresis indicates the first-order nature for the magnetostructural transformation. The entropy changes with a magnetic field variation of 0–5 T are 15.2, 18.8, and 24.3 $J{\cdot}kg^{-1}{\cdot}K^{-1}$ for the $x = 0$, 1, and 2 samples, respectively. The tunable martensitic transformation temperature, enhanced field driving capacity, and large entropy change suggest that $Mn_{48-x}V_xNi_{42}Sn_{10}$ alloys have a potential for applications in magnetic cooling refrigeration.

Keywords: magnetostructural coupling, field driving capacity, refrigeration capacity, magnetocaloric effect

PACS: 75.30.Sg **DOI:** 10.1088/1674-1056/27/3/037504

1. Introduction

Magnetic refrigeration has drawn great attention from researchers because of its advantages over the conventional cooling technique, such as the compact size, low mechanical vibration, environmental friendliness, and high efficiency.[1–3] Materials exhibiting the large magnetic entropy changes (ΔS_M) are potential candidates for magnetic refrigeration applications.[4] Till now, the large ΔS_M has been widely studied in materials experiencing the magnetic-field-induced first-order transition, e.g., La–Fe–Si,[5–7] Gd–Si–Ge,[8] Mn–Fe–P–As,[9] and *M*Mn*X* (*M* = Co or Ni, *X* = Si or Ge) alloys.[10–12] Besides these materials, Heusler-type NiMn-based magnetic shape memory alloys also attract considerable attention for its large and tunable magnetocaloric effect.[13–20]

The magnetocaloric effect in NiMn-based magnetic shape memory alloys is generated from the magnetic-field-induced first-order magnetostructural transformation from martensite to austenite.[21–23] According to Liu's report, the adiabatic temperature change with a magnetic field variation of 0–2 T is as large as −6.2 K in Ni–Mn–In–(Co) alloy,[24] which is larger than the magnetocaloric effect of Gd. Additionally, due to the fact that the magnetostructural transformation temperature is sensitive to the valence electron concentration (e/a),[25] cell volume,[26] grain size,[27] and external parameters (magnetic field or applied hydrostatic pressure),[28] the magnetostructural transformation can be tuned by changing the composition or preparation conditions.[29–35] For instance, the magnetostructural coupling and magnetocaloric effect can be effectively tailored through changing the ratio between Ni and Mn magnetic elements or introducing a fourth magnetic element.[30–32] The doping effect of non-magnetic elements on the magnetostructural transformation and the magnetocaloric properties in Ni–Mn–In alloys has been theoretically studied by Sokolovskiy *et al.*[33] They predicted that the adiabatic temperature change can be enhanced by a factor of 3 when the Mn atoms are partially replaced by non-magnetic Cu atoms in the $Ni_{50}Mn_{34}In_{16}$ alloy.[33] Recently, Kaya *et al.* also reported the improvement of magnetocaloric properties through introducing non-magnetic Al element in the $Ni_{43}Mn_{46}In_{11}$ alloys.[35] Based on these previous experimental and theoretical reports, it is expected that nonmagnetic V element may also be able to tune the magnetostructural transformation and magnetocaloric properties in NiMn-based Heusler alloys.

In this work, we investigate the magnetostructural transformation and magnetocaloric properties of $Mn_{48-x}V_xNi_{42}Sn_{10}$ ($x = 0$, 1, 2, and 3) ferromagnetic shape memory alloys. The martensitic transformation temperature decreases when Mn is substituted by V. High field *M*–*T* and isothermal magnetization curves confirm the magnetic-

*Project supported by the National Natural Science Foundation of China (Grant Nos. 51601092, 51571121, and 11604148), the Fundamental Research Funds for the Central Universities, China (Grant Nos. 30916011344 and 30916011345), the Fund Program for the Scientific Activities of Selected Returned Overseas Professionals in Shanxi Province, China, the Postdoctoral Science Foundation Funded Project (Grant No. 2016M591851), the Natural Science Foundation of Jiangsu Province, China (Grant Nos. BK20160833, 20160829, and 20140035), the Qing Lan Project of Jiangsu Province, the Priority Academic Program Development of Jiangsu Higher Education Institutions, and Shanxi Scholarship Council of China (Grant No. 2016-092).

†Corresponding author. E-mail: xufeng@njust.edu.cn

© 2018 Chinese Physical Society and IOP Publishing Ltd

field-induced magnetostructural transformation. The tunable martensitic transformation temperature, enhanced magnetic field driving capacity, and large magnetic entropy changes are observed.

2. Experiment

The polycrystalline $Mn_{48-x}V_xNi_{42}Sn_{10}$ ($x = 0$, 1, 2, and 3) alloys were prepared by arc melting the appropriate amount of constituents (99.98% purity) in an argon atmosphere using a water-cooled copper crucible. The ingots were remelted for three times to ensure the homogeneity. After that, the ingots were annealed at 1073 K for three days in vacuum quartz tubes, and then quenched into cold water. X-ray energy-dispersive spectroscopy (EDS, Thermo system 7) was used to determine the elemental composition of the samples. The structural transitions were investigated by differential scanning calorimetry (DSC, Mettler Toledo) with a rate of 10 K/min during heating and cooling cycles. The crystal structures of samples were identified by x-ray diffraction (XRD, Bruker, D8 Advance) using Cu-Kα radiations. Magnetic measurements were carried out on physical property measurement system (PPMS, Quantum Design, Dynacool) and magnetic property measurement system (MPMS-7, Quantum Design). To avoid the irreversibility, the isothermal magnetization curves (M–B) were measured using a so-called loop method.[36]

3. Results and discussion

Figure 1 shows the XRD patterns of $Mn_{48-x}V_xNi_{42}Sn_{10}$ ($x = 0$, 1, 2, and 3) alloys at room temperature. For $x = 0$ and 1, a small fraction of martensitic phase is detected in addition to the dominant cubic austenite phase at room temperature. With further increase of x, (022) peak from the martensite shifts to the higher angle and overlaps with the (220) peak from the austenite. It is known that the structure of austenite in Ni–Mn–Sn magnetic shape memory alloy is sensitive to the composition. It could be cubic $L2_1$, Hg_2CuTi, or B2 structure.[37] In this case, the superlattice (111), (222), (400), and (422) reflections confirm $L2_1$ cubic structure. As the size of V (0.134 nm) is larger than that of Mn ($r = 0.126$ nm), with V substitution, the lattice parameter (a) and unit cell volume increase, indicating that V substitution may produce the lattice distortion in these alloys.

Figure 2 shows the DSC curves of $Mn_{48-x}V_xNi_{42}Sn_{10}$ ($x = 0$, 1, 2, and 3) alloys during the heating and cooling processes. The large endothermic/exothermic peaks represent the occurrence of martensitic and reverse martensitic transformations. The thermal hysteresis, which represents the irreversibility between the heating and cooling processes, identifies the first-order nature of the transformation.[38] According to the DSC data, the start and finish temperature of reverse martensitic transformation (A_s and A_f) and the start and finish temperature of martensitic transformation (M_s and M_f) are listed in Table 1. It can be seen that with the V-substitution, the structural transformation temperature (T_t) decreases. Here, T_t in heating (T_t^H) and cooling (T_t^C) processes are defined by $T_t^H = (A_s + A_f)/2$ and $T_t^C = (M_s + M_f)/2$, respectively. The entropy change accompanied with the complete martensitic transformation (ΔS_T) can be determined from the DSC measurements.[39] The estimated values of ΔS_T are 32, 30, 29, and 26 $J \cdot kg^{-1} \cdot K^{-1}$ for $x = 0$, 1, 2, and 3, respectively.

The temperature dependence of magnetization (M–T) curves for $Mn_{48-x}V_xNi_{42}Sn_{10}$ ($x = 0$, 1, and 2) alloys were

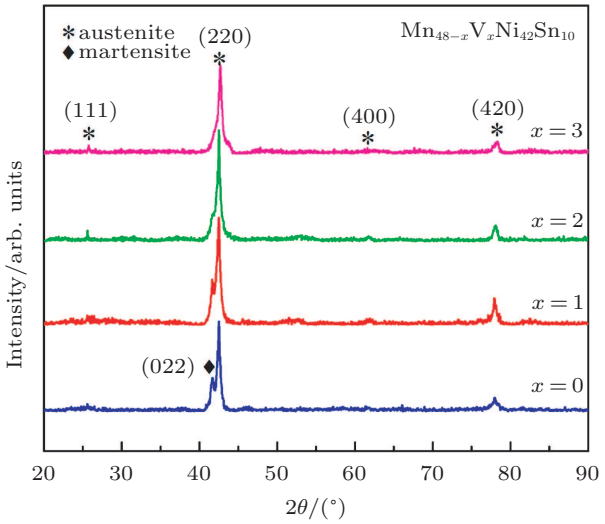


Fig. 1. (color online) XRD patterns of $Mn_{48-x}V_xNi_{42}Sn_{10}$ ($x = 0$, 1, 2, and 3) alloys at room temperature.

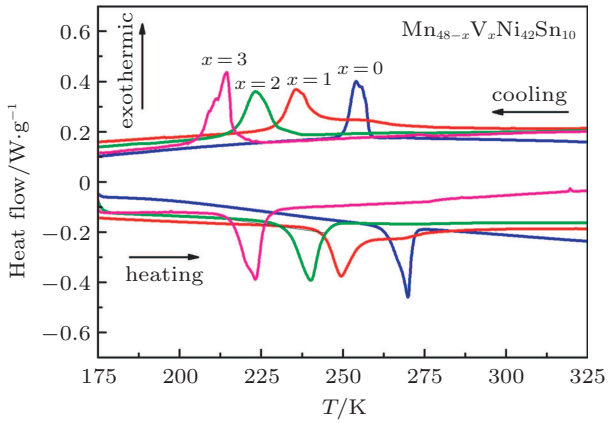


Fig. 2. (color online) DSC curves of $Mn_{48-x}V_xNi_{42}Sn_{10}$ ($x = 0$, 1, 2, and 3) alloys during heating and cooling processes.

Table 1. The measured elemental compositions and corresponding electronic concentrations for the present $Mn_{48-x}V_xNi_{42}Sn_{10}$ ($x = 0$, 1, 2, and 3) samples.

x	Mn/at.%	Ni/at.%	Sn/at.%	V/at.%	e/a
0	47.88	42.17	9.95	00	7.961
1	46.85	42.09	9.91	1.15	7.942
2	45.90	42.11	10.07	1.92	7.923
3	44.88	42.16	10.11	2.85	7.904

measured to investigate the magnetic phase transitions. Figure 3 shows the M–T curves of $Mn_{48-x}V_xNi_{42}Sn_{10}$ ($x = 0$, 1, and 2) alloys under an applied field of 0.01 T. With increasing the temperature, all the samples transform from a weak magnetic martensite to a ferromagnetic austenite, as shown in Fig. 3. A thermal hysteresis of about 11 K is observed for all the three samples accompanied with the martensitic transformation, indicating the first-order nature for the magnetostructural transformation. The estimated values of A_s, A_f, M_s, M_f, T_t^H, and T_t^C from M–T curves are listed in Table 2. These characteristic temperatures for the transitions from the M–T curves agree well with the DSC measurement (Fig. 2). It is known that T_t is related to the value of e/a.[31] In this case, e/a decreases with the substitution of V for Mn, as T_t decreases. Additionally, T_t in NiMn-based magnetic shape memory alloy is also sensitive to the cell volume. The partial replacement of Mn by V atoms induces the expansion of the unit cell, which also shifts the magnetostructural transformation to lower temperatures.

In order to investigate the magnetic-field-induced structural transformation, the isothermal magnetization (M–B) curves for $Mn_{48-x}V_xNi_{42}Sn_{10}$ ($x = 0$, 1, and 2) alloys in the field of 0–5 T were measured by the so-called loop method.[36] Initially the samples were cooled down to complete the martensitic state and then slowly heated to the target temperature before starting each M–B measurement. As shown in Figs. 4(a)–4(c), the curves show an obvious metamagnetic behavior around T_t, which corresponds to the magnetic-field-induced structural transformation from a week magnetic martensite to a ferromagnetic austenite. The magnetic hysteresis reflects the first-order nature of the transition. The values of magnetization difference (ΔM) under the field of 5 T are 41.6, 43.9, and 46.7 Am^2/kg for $x = 0$, 1, and 2, respectively. The increase of ΔM in $Mn_{46}V_2Ni_{42}Sn_{10}$ is attributed to the enhanced field driving capacity.

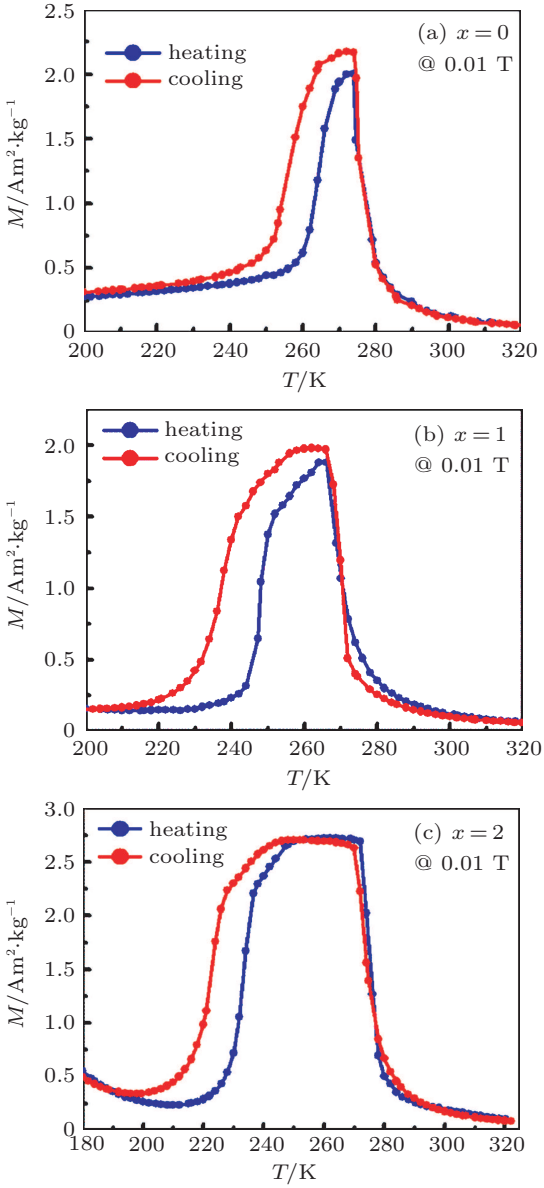


Fig. 3. (color online) The temperature dependence of magnetization (M–T) curves for $Mn_{48-x}V_xNi_{42}Sn_{10}$ ($x = 0$, 1, and 2) alloys under an applied field of 0.01 T. (a) $x = 0$, (b) $x = 1$, and (c) $x = 2$.

Table 2. Phase transformation temperatures, effective refrigeration capacity (RC_{eff}), field driving capacity (dT/dB), and magnetic entropy change (ΔS_M) for the $Mn_{48-x}V_xNi_{42}Sn_{10}$ ($x = 0$, 1, and 2) alloys.

Sample	A_s /K	A_f /K	M_s /K	M_f /K	T_t^H /K	T_t^C /K	dT_t/dB /K· T^{-1}	RC_{eff} /J· kg^{-1}	$\Delta S_M(\Delta B = 5$ T) /J· kg^{-1}· K^{-1}
$x = 0$	261	268	259	251	266	256	−1.4	37.21	15.2
$x = 1$	245	254	242	233	249	237	−1.7	75.4	18.8
$x = 2$	231	238	288	218	235	223	−2.01	82	24.3

Owing to the magnetization difference between the martensite and austenite, the structural transformation can be driven by the magnetic field. With increasing the magnetic field from 3 to 5 T, the M–T curves of $Mn_{48-x}V_xNi_{42}Sn_{10}$ ($x = 0$, 1, and 2) alloys shift to the lower temperature, as shown in Fig. 4(d). The rate of A_s shifted by magnetic field, i.e., dA_s/dB, is −1.4, −1.7, and −2.01 K·T^{-1} for the $x = 0$, 1, and 2 samples, respectively, confirming the field-induced magnetostructural transformation. The enhanced magnetic field driving capacity with the V-substitution in $Mn_{48-x}V_xNi_{42}Sn_{10}$ ($x = 0$, 1, and 2) alloys can be attributed to the larger magnetization difference. It is also well known that the maximum value of magnetic entropy change (ΔS_M) can be estimated by M–T curves measured at different constant fields. We calculated the ΔS_M value for $Mn_{46}V_2Ni_{42}Sn_{10}$ alloy using Clausius–Clapeyron equation

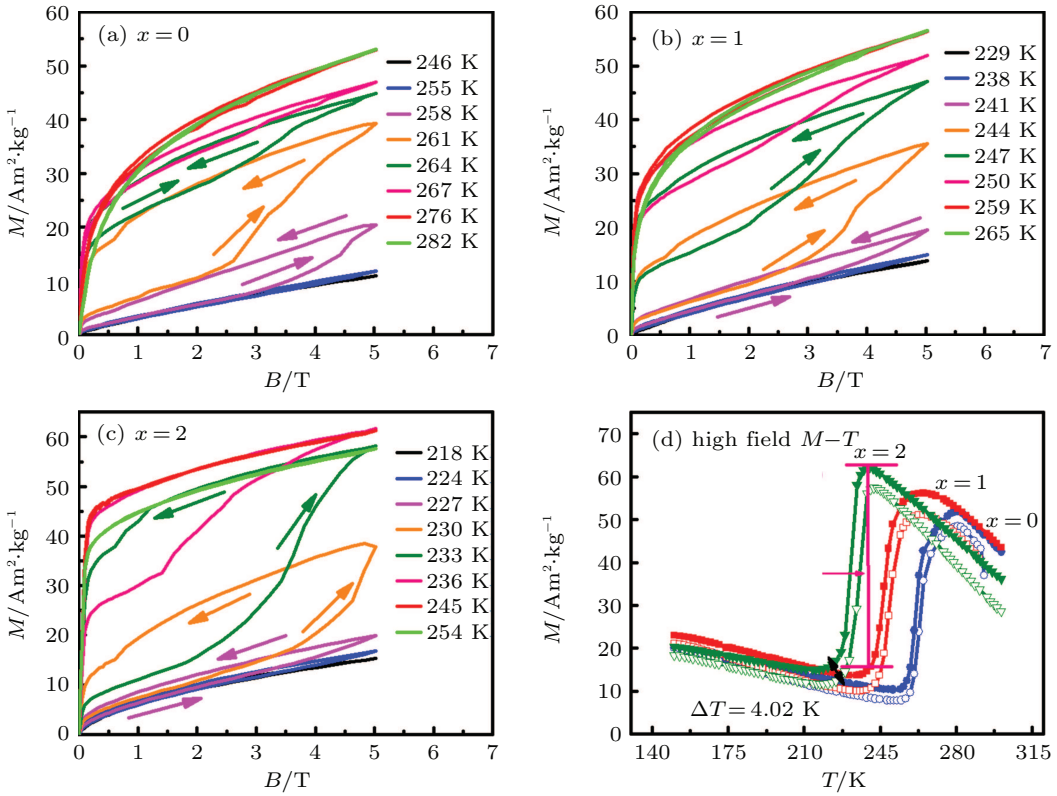


Fig. 4. (color online) M–B curves at various temperatures around the martensitic transformation for the $Mn_{48-x}V_xNi_{42}Sn_{10}$: (a) $x = 0$, (b) $x = 1$, and (c) $x = 2$. (d) High field M–T curves for $Mn_{48-x}V_xNi_{42}Sn_{10}$ ($x = 0$, 1, and 2) alloys with a magnetic field of 3 T (open symbols) and 5 T (solid symbols) in the heating process.

($\Delta S = -\Delta M \cdot \mathrm{d}B/\mathrm{d}T$) from M–T curves at 3 and 5 T, as shown in Fig. 4(d). The calculated maximum value of ΔS is 23.3 J·K^{-1}·kg^{-1} (using $\Delta M = 47.23$ Am^2/kg, $\Delta B = 2$ T, and $\Delta T = 4.02$ K), and it is in a good agreement with that obtained from M–B curves using Maxwell relations.

According to the M–B curves, the ΔS_{M} during the magnetic-field-induced structural transformation is calculated by Maxwell relation

$$\Delta S_{\mathrm{M}} = \int_0^B \frac{\delta M(B,T)}{\delta T}\,\mathrm{d}B. \tag{1}$$

The temperature dependence of ΔS_{M} with a magnetic field variation of 0–5 T for $Mn_{48-x}V_xNi_{42}Sn_{10}$ ($x = 0$, 1, and 2) alloy is shown in Fig. 5. The maximum values for ΔS_{M} are 15.2, 18.8, and 24.3 J·kg^{-1}·K^{-1} for $x = 0$, 1, and 2, respectively, which are smaller than ΔS_{T} derived from the DSC measurements. The low ΔS_{M} derived from Maxwell relation originates from the incomplete phase transition driven by a magnetic field of 5 T, as shown in Figs. 4(a)–4(c). The large values of ΔS_{M} for $Mn_{48-x}V_xNi_{42}Sn_{10}$ are comparable with other magnetocaloric materials experiencing a first-order transition, such as $Ni_{48-x}Co_2Mn_{38+x}Sn_{12}$, $Mn_{50}Ni_{40-x}Co_xSn_{10}$, $Mn_{50}Ni_{40}Sn_{10-x}Sb_x$, $Mn_{1-x}Al_xCoGe$, and $Mn_{1+x}Co_{1-x}Ge$ alloys.[39–44] It is known that the value of ΔS_{M} in a material that experiences the magnetic-field-induced magnetostructural transformation is highly related to the sharp variation in magnetization between austenite and martensite. In NiMn-based magnetic shape memory alloys, the magnetization is mainly induced by the Mn atoms and very sensitive to the Mn–Mn distance. As a result, a small variation in Mn atoms may cause lattice distortion in these alloys. The large values of ΔM are attributed to two different interaction mechanisms: one is the strong spin–phonon interaction which leads the different magnetic states between two phases, while the other one is magnetostructural coupling, resulting in the large magnetization jump around martensitic transformation.

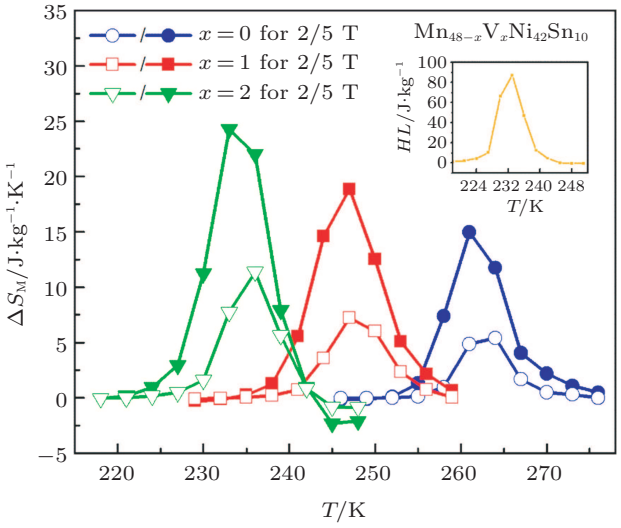


Fig. 5. (color online) The temperature dependence of ΔS_{M} under an applied magnetic field of 2 and 5 T for $Mn_{48-x}V_xNi_{42}Sn_{10}$ ($x = 0$, 1, and 2) alloys measured upon heating. Inset: HL of $Mn_{46}V_2Ni_{42}Sn_{10}$ alloy.

The effective refrigeration capacity ($RC_{\rm eff}$) of $Mn_{48-x}V_xNi_{42}Sn_{10}$ ($x = 0$, 1, and 2) alloys is calculated by subtracting the average hysteresis loss (HL) from the refrigeration capacity (RC) values. Here, the value of RC is obtained by integrating the area under $\Delta S_{\rm M}$–T curves using the temperature at half maximum of the peak as the integration limits.[38] The average HL is calculated by the method mentioned in Ref. [45]. The temperature dependence of HL for $Mn_{46}V_2Ni_{42}Sn_{10}$ alloy is shown as the inset of Fig. 5. The values of $RC_{\rm eff}$ around the temperature of martensitic transformation under the field change of 0–5 T are 37.21, 75.4, and 82 J·kg^{-1} for $x = 0$, 1, and 2, respectively. Consequently, the substitution of V for Mn leads to an increase in the magnetization jump at the magnetostructural transition, the enhanced magnetic field driving capacity ($\mathrm{d}A_{\rm s}/\mathrm{d}B$), and effective refrigeration capacity ($RC_{\rm eff}$).

4. Conclusion

The magnetostructural transformation and the coupled magnetocaloric properties for $Mn_{48-x}V_xNi_{42}Sn_{10}$ ($x = 0$, 1, 2, and 3) ferromagnetic shape memory alloys are investigated using both structural and magnetization measurements. By replacing Mn with V, the martensitic transformation temperature can be tuned within a wide temperature range. The magnetic-field-induced magnetostructural transformation is confirmed by the high field M–T curves and isothermal magnetization curves. The observed peak values of $\Delta S_{\rm M}$ under an applied magnetic field of 5 T for $x = 0$, 1, and 2 are 15.2, 18.8, and 24.3 J·kg^{-1}·K^{-1}, respectively. Large values of $\Delta S_{\rm M}$, enhanced field driving capacity, and tunable martensitic transformation temperatures suggest that $Mn_{48-x}V_xNi_{42}Sn_{10}$ ($x = 0$, 1, 2, and 3) alloys are promising candidates for magnetic refrigeration applications.

References

[1] Fang Y K, Yeh C C, Chang C W, Chang W C, Zhu M G and Li W 2007 *Scr. Mater.* **57** 45
[2] Morrison K, Miyoshi Y and Moore J D 2008 *Phys. Rev. B* **78** 134418
[3] Sandeman K G 2012 *Scr. Mater.* **67** 566
[4] Hu F X, Shen B G, Sun J R, Cheng Z H, Rao G H and Zhang X X 2001 *Appl. Phys. Lett.* **78** 3675
[5] Lyubina J, Nenkov K, Schultz L and Gutfleisch O 2008 *Phys. Rev. Lett.* **101** 177203
[6] Zhang H, Sun Y J, Li Y I, Wu Y Y, Long Y, Shen J, Hu F X, Sun J R and Shen B 2015 *J. Appl. Phys.* **117** 063902
[7] Mandal K and Pal D 2007 *J. Appl. Phys.* **102** 053906
[8] Pecharsky V K and Gschneidner Jr K A 1997 *Phys. Rev. Lett.* **78** 4494
[9] Tegus O, Brück E, Buschow K H J and de Boer F R 2002 *Nature* **415** 150
[10] Hassan N U, Chen F, Zhang M, Shah I A, Liu J, Gong Y Y, Xu G and Xu F 2017 *J. Magn. Magn. Mater.* **439** 120
[11] Sandeman K G, Daou R, Özcan S, Durrell J H, Mathur N D and Fray D J 2006 *Phys. Rev. B* **74** 22443
[12] Liu E K, Wang W H, Feng L, Zhu W, Li G J, Chen J L, Zhang H W, Wu G H, Jiang C B, Xu H B and de Boer F R 2012 *Nat. Commun.* **3** 873
[13] Ullakko K, Huang J K, Kantner C, O'Handley R C and Kokorin V V 1996 *Appl. Phys. Lett.* **69** 1966
[14] Khan N, Ali N and Stadler S 2007 *J. Appl. Phys.* **101** 053919
[15] Liu Z H, Aksoy S and Acet M 2009 *J. Appl. Phys.* **105** 033913
[16] Han Z D, Wang D H, Zhang C L, Xuan H C, Zhang J R, Gu B X and Du Y W 2008 *J. Appl. Phys.* **104** 053906
[17] Planes A, Osa L M, Moya X, Krenke T, Acet M and Wassermann E F 2007 *J. Magn. Magn. Mater.* **310** 2767
[18] Wang D H, Han Z D, Xuan H C, Ma S C, Chen S Y, Zhang C L and Du Y W 2013 *Chin. Phys. B* **22** 077506
[19] Li P P, Wang J M and Jiang C B 2011 *Chin. Phys. B* **20** 028104
[20] Tian L G, Hong L Z, Yan M F, Qiao M X and Heng W G 2013 *Chin. Phys. B* **22** 126201
[21] Han Z D, Wang D H, Zhang C L, Xuan H C, Zhang J R, Gu B X and Du Y W 2008 *Solid State Commun.* **146** 124
[22] Sutou Y, Imano Y, Koeda N, Omori T, Kainuma R, Ishida K and Oikawa K 2004 *Appl. Phys. Lett.* **85** 198
[23] Bhobe P A, Priolkar K R and Nigam A K 2007 *Appl. Phys. Lett* **91** 242503
[24] Liu J, Gottschall T, Skokov K P, Moore J D and Gutfleisch O 2012 *Nat. Mater.* **11** 620
[25] Krenke T, Acet M and Wassermann E F 2005 *Phys. Rev. B* **72** 014412
[26] Karaman I, Basaran B, Karaca H E, Karsilayan A I and Chumlyakov Y I 2007 *Appl. Phys. Lett.* **90** 172505
[27] Wu R, Shen F, Hu F, Wang J, Bao L, Zhang L, Liu Y, Zhao Y, Liang F, Zuo W, Sun J and Shen B 2016 *Sci. Rep.* **6** 20993
[28] Chatterjee S, Giri S and Majumdar S 2008 *Phys. Rev. B* **77** 012404
[29] Samanta T, Dubenko I, Quetz A, Stadler S and Ali N 2012 *Appl. Phys. Lett.* **101** 242405
[30] Sharma V K, Chattopadhyay M K and Roy S B 2007 *J. Phys. D-Appl. Phys.* **40** 1869
[31] Han Z D, Wang D H, Zhang C L, Xuan H C, Gu B X and Du Y W 2007 *Appl. Phys. Lett.* **90** 042507
[32] Han Z D, Wang D H, Zhang C L, Tang S L, Gu B X and Du Y W 2006 *Appl. Phys. Lett.* **89** 182507
[33] Sokolovskiy V V, Buchelnikov V D, Taskaev S V, Khovaylo V V, Ogura M and Entel P 2013 *J. Phys. D-Appl. Phys.* **46** 305003
[34] Moya X, Mañosa L, Planes A, Aksoy S and Acet M 2007 *Phys. Rev. B* **75** 184412
[35] Kaya M, Cicek M M, Dincer I and Elerman Y 2017 *J. Magn. Magn. Mater.* **442** 429
[36] Caron L, Oub Z Q, Nguyen T T, CamThanh D T, Tegus O and Brűck E 2009 *J. Magn. Magn. Mater.* **321** 3559
[37] Graf T, Felser C and Parkin S S P 2011 *Prog. Solid State Chem.* **39** 1
[38] Liu J, Gong Y Y, Xu G Z, Peng G, Shah I A, Hassan N U and Xu F 2016 *Sci. Rep.* **6** 23386
[39] Rama Rao N V, Chandrasekaran V and Suresh K G 2010 *J. Appl. Phys.* **108** 043913
[40] Shah I A, Hassan N U, Rauf A, Liu J, Gong Y Y, Xu G and Xu F 2017 *Chin. Phys. B* **26** 097501
[41] Sharma J and Suresh K G 2015 *J. Alloys Compd.* **620** 329
[42] Shah I A, Hassan N U, Liu J, Gong Y Y, Xu G and Xu F 2017 *Chin. Phys. B* **26** 017501
[43] Aryal A, Quetz A, Pandey S, Samanta T, Dubenko I, Hill M, Mazumdar D, Stadler S and Ali N 2017 *J. Alloys Compd.* **709** 142
[44] Ma S C, Wang D H, Xuan H C, Shen L J, Cao Q Q and Du Y W 2011 *Chin. Phys. B* **20** 087502
[45] Lai J W, Zheng Z G, Zhong X C, Montemayor R, Liu Z W and Zeng D C 2015 *Intermetallics* **63** 7